

Cascade Control of Single Input Multi Output Buck Converter for Synchronous Charging Applications of Battery/Ultracapacitor Hybrid Energy Storage Systems

Muhammed Reşit ÇORAPSIZ^{1*} 

¹ Erzurum Technical University, Faculty of Engineering and Architecture, Department of Electrical & Electronics Engineering, Erzurum, Türkiye
Muhammed Reşit ÇORAPSIZ ORCID No: 0000-0001-5477-5299

*Corresponding author: r.corapsiz@erzurum.edu.tr

(Received: 04.11.2024, Accepted: 24.01.2025, Online Publication: 26.03.2025)

Keywords

Li-ion batteries,
Ultra-capacitor,
Hybrid energy storage
systems,
Multi-output DC-DC
converters,
Hybrid charging systems

Abstract: In the near future, seeing more than one energy storage device in mobile device power systems will be possible. In today's technology, although Lithium-ion (Li-ion) battery cells stand out with their high energy density and superior cell voltage advantages, they suffer from limited cycle lives. A highly efficient hybrid power system can be created when high-power density ultracapacitors (UC) are combined with battery cells. However, since the cell voltages and power densities of these two energy storage devices are not equal, both the charge voltages and charge currents will be different from each other. This study proposes a single-input, multi-output cascade buck converter structure to synchronously charge battery and ultracapacitor cells. Converter parameters are calculated according to the charge powers of energy storage devices, and a cascade controller structure is designed to control charge current and cell voltage separately. The proposed synchronous charging system is tested using two different procedures: constant current (CC) mode, where reference currents are closely monitored, and constant voltage (CV) mode, where the charge voltage is limited. According to the results obtained, it was observed that the proposed system closely followed the reference currents in a short time of 6ms with a slight overshoot rate of approximately 8% in all tests.

103

Pil/Ultrakapasitör Hibrit Enerji Depolama Sistemlerinin Senkron Şarj Uygulamaları İçin Tek Girişli Çok Çıkışlı Düşürücü Dönüştürücünün Kademeli Kontrolü

Anahtar Kelimeler

Lityum-iyon piller, Ultra-
kapasitör, Hibrit enerji
depolama sistemleri,
Çok çıkışlı DC-DC
dönüştürücüler,
Hibrit şarj sistemleri

Öz: Yakın gelecekte, mobil cihaz güç sistemlerinde birden fazla enerji depolama aygıtı görmek mümkün olacaktır. Günümüz teknolojisinde Lityum-iyon (Li-ion) pil hücreleri yüksek enerji yoğunluğu ve üstün hücre voltajı avantajlarıyla öne çıksa da sınırlı çevrim ömürlerinden muzdariptir. Yüksek güç yoğunluklu ultra kapasitörler (UC) pil hücreleriyle birleştirildiğinde, oldukça verimli bir hibrit güç sistemi oluşturulabilir. Ancak, bu iki enerji depolama aygıtının hücre voltajları ve güç yoğunlukları eşit olmadığından hem şarj voltajları hem de şarj akımları birbirinden farklı olacaktır. Bu çalışmada, pil ve ultra kapasitör hücrelerini senkron olarak şarj etmek için tek girişli, çok çıkışlı bir kademeli düşürücü dönüştürücü yapısı önerilmiştir. Dönüştürücü parametreleri, enerji depolama aygıtlarının şarj güçlerine göre hesaplanmış ve şarj akımlarının ve hücre voltajlarının ayrı ayrı kontrolü için bir kademeli denetleyici yapısı tasarlanmıştır. Önerilen senkron şarj sistemi, referans akımlarının yakından izlendiği sürekli akım (CC) modu ve şarj voltajının sınırlandırıldığı sürekli voltaj (CV) modu olmak üzere iki farklı prosedür kullanılarak test edilmiştir. Elde edilen sonuçlara göre önerilen sistemin tüm testlerde yaklaşık %8'lik hafif bir aşma oranıyla 6ms gibi kısa bir sürede referans akımlarını yakından takip ettiği gözlenmiştir.

1. INTRODUCTION

Governments and countries' global economic growth targets and the increased industrialization rate have caused a significant increase in energy consumption levels in recent years [1, 2]. The development of energy storage systems has an active role in spreading portable electronic devices and advancing minimum carbon footprint targets [3-5]. The energy and power capacities of energy storage devices are very important for the sustainability of these systems. In addition to these critical features, power converters provide bidirectional power flow from energy storage devices to the load side and from the load side to the energy storage devices [6]. Power electronic converters are frequently used in renewable energy systems due to the constant DC bus voltage required for high power quality [7-9]. As is known, the cell voltages of energy storage devices (e.g., battery or ultracapacitor cells) decrease over time in the discharge state [10]. This situation continues up to a specific cut-off voltage in battery cells. In contrast, the terminal voltage of an ultracapacitor can continue till close to zero depending on the discharge current amplitude in the ultracapacitor cell. Power electronic converters are designed not to reflect this change on the load side. In addition, since the terminal voltages and discharge capacities of the mentioned energy storage cells are limited, series and parallel connection of these devices may not meet this demand in loads that require high supply voltage or high supply current. In energy storage systems, if the terminal voltage on the source side is greater than the supply voltage on the load side, buck converters (conventional buck [11], quadratic buck [12], buck-boost [13], etc.) are used. If the supply voltage on the load side is greater than the terminal voltage on the source side, boost converters (conventional boost [14], Cuk [15], SEPIC [16], buck-boost, etc.) are used to equalize the source-load potential. Energy storage devices should be charged with a limited terminal current generated at a limited terminal voltage. These limited values are usually provided by the manufacturer. These values should not be exceeded during the charging and discharging processes for long-term use and safe operation of the devices [17]. Therefore, in an energy storage system designed using power converters, only averaged voltage mode control or averaged current mode control may not fully meet a high-performance and high-security charging process. As a result, separate control of the charging voltage and charging current is essential for performance and efficiency, especially safety in energy storage devices. In [12], a second-order buck converter was proposed as a competitive alternative to battery charging systems. In the study where the cascade control technique was used in charge control, a constant current constant voltage (CC-CV) charging protocol was adopted using three control loops. This protocol is the most common method for charging battery cells or packs. In [18] a bidirectional buck-boost converter was used to provide power from the sources to the vehicle drive system and store regenerative braking currents for electric vehicles consisting of battery and supercapacitor packs. A fully active topology structure was used in the study, and a two-stage control technique was applied over the

inductor current and DC bus voltage. However, the external charging states of the battery and supercapacitor packs were not examined. Most studies on energy storage systems consisting of battery and supercapacitor packs have focused on efficiently sharing energy and power between these two sources [19-21]. In systems with hybrid energy storage units, the charging conditions of the devices are as important as the effective power sharing between the devices. Especially in electric vehicles containing battery and supercapacitor packs, the state of charge (SoC) of the battery and supercapacitor packs may differ after a specific driving cycle [22]. This is usually due to the power-sharing technique adopted in energy management. In addition, the different energy and power densities of the devices are another factor affecting the SoC difference [23]. It has been reported that operating lithium-ion batteries, which are frequently used in electric vehicles, in the 10% – 70% SoC range positively affects battery health and life [24]. This range can be used for much more expansive limits for ultracapacitor packs. However, ultracapacitors used in hybrid energy storage systems are generally preferred to protect the battery packs from high currents during charging and discharging [25]. Therefore, the supercapacitor packs in these systems should be operated in a SoC range that can provide power to the load at any time on demand and store the recovered energy from the load at any time [26]. Considering these critical limits, at the end of a certain driving cycle for electric vehicles or the end of a certain load supply for energy storage systems, the battery and ultracapacitor must be charged to meet the next load requirements. The charging process can be carried out in three ways: *i*) While the battery group is charged, the ultracapacitor group can be charged using only the recovered energy, considering it operates within a specific SoC range, *ii*) After the battery group is charged, the charging requirement of the ultracapacitor group can be provided by the battery group with the help of a power converter. Both techniques mentioned above can extend the charging time of the ultracapacitor group, shorten the battery usage time, and negatively affect the system's efficiency. *iii*) The battery and ultracapacitor group can charge synchronously via a cascade-connected power converter. Thus, the battery and ultracapacitor groups are charged to the determined maximum SoC level at the end of the charging process. The third step emphasizes the main contribution of this study. A new technique based on synchronous charging of both battery and ultracapacitor packs via a single-input multi-output buck converter is proposed to make a critical contribution to this process. The proposed synchronous charging technique will prevent the negatives mentioned in *i*) and *ii*) since it will charge the battery and ultracapacitor packs simultaneously. Thus, the ultracapacitor can provide the necessary power at any time and store the necessary energy.

The present paper is organized as follows. Section 2 and Section 3 explain the energy storage principles and electrical equivalent circuits of Li-ion battery and ultracapacitor cells, respectively. Section 4 examines the structure, design and control of the cascade buck converter in detail. Results and discussion are presented

in Section 5, while Section 6 includes the main findings of this study.

2. LITHIUM-ION (LI-ION) BATTERIES

Critical features such as high energy density, long service life, wide operating temperature range, and low self-discharge are desired in batteries used in energy storage systems [27]. Among these critical features, energy density affects the energy supply time of the battery, while service life refers to the service period until the battery reaches the end of life (EoL). It is generally assumed that a battery cell has reached EoL when it has lost 20% of its initial capacity [28]. The battery cell must have high SoC retention capability and low self-discharge under negative temperature conditions, especially in electric vehicles with battery/ultracapacitor packs located in regions with intense winter conditions or in energy storage systems. Considering the features explained above, Lithium-ion batteries, which have these critical advantages, are frequently preferred in today's technology in electric vehicles and energy storage systems. Figure 1 represents the internal structure of a Li-ion battery cell [29].

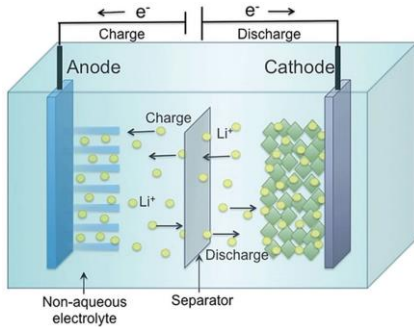


Figure 1. Behavior of a Lithium-ion battery (LiB) under charge and discharge conditions

Lithium-ion batteries, commercialized by SONY in the last quarter of the 20th century, consist of a lithium metal oxide cathode, an electrolyte made of lithium salt, and a graphite anode [30]. In addition, a separator in the electrolyte prevents the electron transfer from the anode to the cathode during charging and from the cathode to the anode during discharging. In a commercialized Li-ion battery cell, the cathode is usually coated on a copper layer and the anode on an aluminum layer. The positively charged Li⁺ ions are attracted to the negative terminal when the cell is charged. During this time, the electrons flow in the opposite direction of the current path and pass to the cathode region. The cell is said to be fully charged when this process is completed. During the discharge process, this reaction occurs oppositely. An electrical equivalent circuit can usually represent this complex electrochemical transformation. The Li-ion battery cell in MATLAB/Simulink Simscape/Electrical was used for the simulation tests in this study. This cell uses the Shepherd electrical equivalent circuit model shown in Figure 2.

The Shepherd battery model in Figure 2 is shown among the best-known electrical equivalent circuit models, and the relationships in the charge-discharge state are given as follows [31].

$$v_{bat} = E_{bat} - R_{bat}i_{bat} \quad (1)$$

$$E_{ch} = E_0 - K \left(\frac{Q}{it + 0.1Q} \right) i^* - K \left(\frac{Q}{Q - it} \right) it - R_{bat}i + Ae^{-B \cdot it} \quad (2)$$

$$E_{disch} = E_0 - K \left(\frac{Q}{Q - it} \right) i^* - K \left(\frac{Q}{Q - it} \right) it - R_{bat}i + Ae^{-B \cdot it} \quad (3)$$

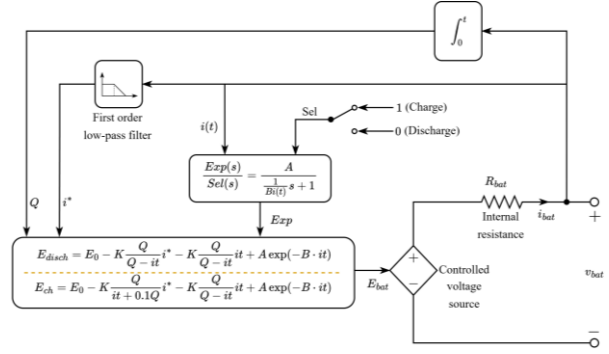


Figure 2. Shepherd battery model

In the notations in Equations 1-3, E_{disch} and E_{ch} represent the discharge and charge voltages (V), E_0 is the open circuit voltage (OCV) (V), V_{bat} is the battery terminal voltage (V), K is the polarization resistance coefficient (Ω), Q is the battery capacity (Ah), i_{bat} is the battery current (A), i^* is the filtered battery current (A), R_{bat} is the battery internal resistance (Ω), t is the time (h), A , B are empirical constants (V), (1/Ah), respectively. While the inside of the i^* term in Equation 3 represents the polarization resistance, the inside of the it term represents the polarization voltage. The parameters E_0 , R_{bat} , K , A , B in Equations 2 and 3 are determined using the nominal voltage (V) and rated capacity (Ah) values. In this model, the ampere-hour counting technique given in Equation 4 is used to determine the battery state of charge (SoC).

$$SoC_{bat} = SoC_{init-bat} - \frac{1}{3600 * Q} \int i_{bat} dt \quad (4)$$

In this study, a single cell known as the cylindrical 18650 model, which many battery manufacturers commercialize, is used to perform the proposed synchronous charging process. Various electrical characteristics of this cell are given in Table 1.

Table 1. Electrical parameters of the battery cell

Parameter	Description	Value	Unit
R_{bat}	Internal resistance	14.4	m Ω
V_{bat}	Nominal voltage	3.6	V
Q_{rated}	Rated Capacity	2.5	Ah
$V_{cut-off}$	Cut-off voltage	2.7	V
V_{full}	Fully charged voltage	4.19	V
I_{a-nom}	Nominal discharge current	1.087	A
$SoC_{init-bat}$	Initial state of charge	50(%)	-

The electrical parameters given in Table 1 were determined by considering the values of a commercialized

battery cell. These battery parameters can be found in the following reference [32].

3. ULTRACAPACITORS

The limited power density, limited cycle life, and limited charge and discharge currents of battery technologies used in energy storage systems can cause range problems in electric vehicles and intermittent power flow in grid-connected systems. Since battery groups convert chemical energy into electrical energy, they have slow dynamics due to a series of chemical reactions. In addition, the lithium inventory loss (LLI) during each charge and the active material loss (LAM) that arises depending on the number of cycles limit the battery service life. Therefore, using ultracapacitors with high power density and cycle life [33], and can withstand sudden current changes in energy storage systems containing battery packs has contributed to solving the abovementioned problems. Another feature of ultracapacitors is that they can store energy produced from intermittent renewable energy sources (e.g., wind and solar) or high regenerative currents occurring in electric vehicles.

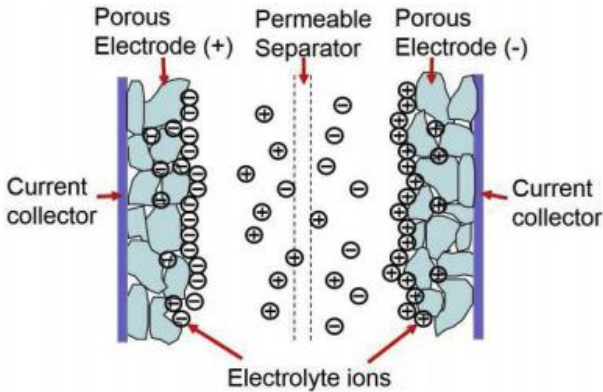


Figure 3. Structure of an ultracapacitor in the charged state

A schematic diagram of an ultracapacitor in the charged state is shown in Figure 3 [34]. An ultracapacitor or electric double layer capacitor (EDLC) consists of two porous electrodes, two electrolytes, a separator, and a current collector. Since the porous electrodes increase the surface area, these devices can be manufactured up to thousands of Farads. The capacitance of an ultracapacitor is similar to that of conventional capacitors and can be given as follows.

$$C_{UC} = \frac{\epsilon_r \epsilon_0 A}{d} \quad (5)$$

In Equation 5, C represents the capacitance of the ultracapacitor, ϵ_r is the dielectric constant of the electrolyte, ϵ_0 is the dielectric constant of the vacuum, d is the effective thickness of the double layer, and A is the accessible surface area. In addition, the separator immersed in the electrolyte prevents electrical contact between the electrodes [35]. The energy stored in an ultracapacitor is given as follows:

$$W_{uc} = \frac{1}{2} C_{uc} V_{uc}^2 \quad (6)$$

In Equation 6, W_{uc} represents the amount of stored energy, C_{uc} represents the capacitance, and V_{uc} represents the terminal voltage. As in battery applications, ultracapacitors can also be represented by electrical equivalent circuit models. The Zubieta model [36] is often preferred among these equivalent circuits, as it provides close values in both simulation and experimental applications.

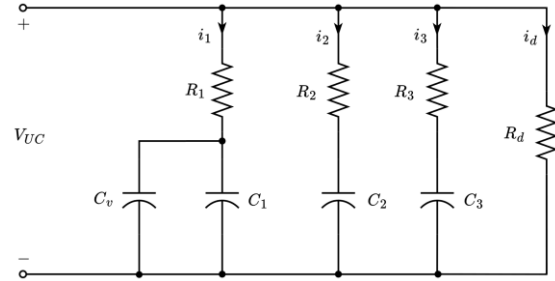


Figure 4. Zubieta ultracapacitor model

In the notations in Figure 4, C_1 , C_2 , and C_3 represent fixed capacitances, and C_v represents voltage-dependent capacitance (Differential capacitance). R_1 , R_2 , and R_3 represent fixed resistances, R_d represents self-discharge resistance, i_1 , i_2 , i_3 , and i_d represent the branch current to which they are connected. To represent the voltage-dependent capacitance gain K_v , the i_1 current in the electrical equivalent circuit can be expressed as follows depending on the voltage (V_{C_1}) between the C_v and C_1 capacitors.

$$i_1 = (C_1 + K_v V_{C_1}) \frac{dV_{C_1}}{dt} \quad \text{if } V_{C_1} > 0 \quad (7)$$

$$i_1 = C_1 \frac{dV_{C_1}}{dt} \quad \text{if } V_{C_1} < 0 \quad (8)$$

The currents of the second and third branches can be determined by $i_n = C_n \frac{dV_{C_n}}{dt}$, $\{n \in \{2, 3\}\}$. The SoC of the ultracapacitor is directly proportional to the terminal voltage and can be determined as follows.

$$SoC_{uc} = \frac{Q_{init-uc}}{C_{uc} V_{uc}} \int i_{uc} dt \quad (9)$$

The electrical properties of the cylindrical model ultracapacitor cell for the synchronous charging process proposed in this study are given in Table 2.

Table 2. Electrical parameters of the ultracapacitor cell

Parameter	Description	Value	Unit
R_{ESR}	Equivalent series resistance	8.9	mΩ
V_{rated}	Rated voltage	2.7	V
C_{rated}	Rated Capacity	30	F
V_{init}	Initial voltage	1.5	V
$SoC_{init-uc}$	Initial state of charge	49.5(%)	-

The electrical parameters given in Table 2 were determined by considering the values of a commercialized

ultracapacitor cell. These ultracapacitor parameters can be found in the following reference [37].

4. BUCK CONVERTER

DC-DC converters are power electronic devices used to meet load requirements with different voltage and current levels. Buck converters with low voltage gain can

theoretically change the voltage applied from the input stage to the output stage between zero and the input voltage thanks to the appropriate switch duty ratio ($d = V_o/V_s$). For this reason, they are widely used in mobile devices, wearable technologies, battery applications, electric vehicles, and energy harvesting systems where low voltage is required [38].

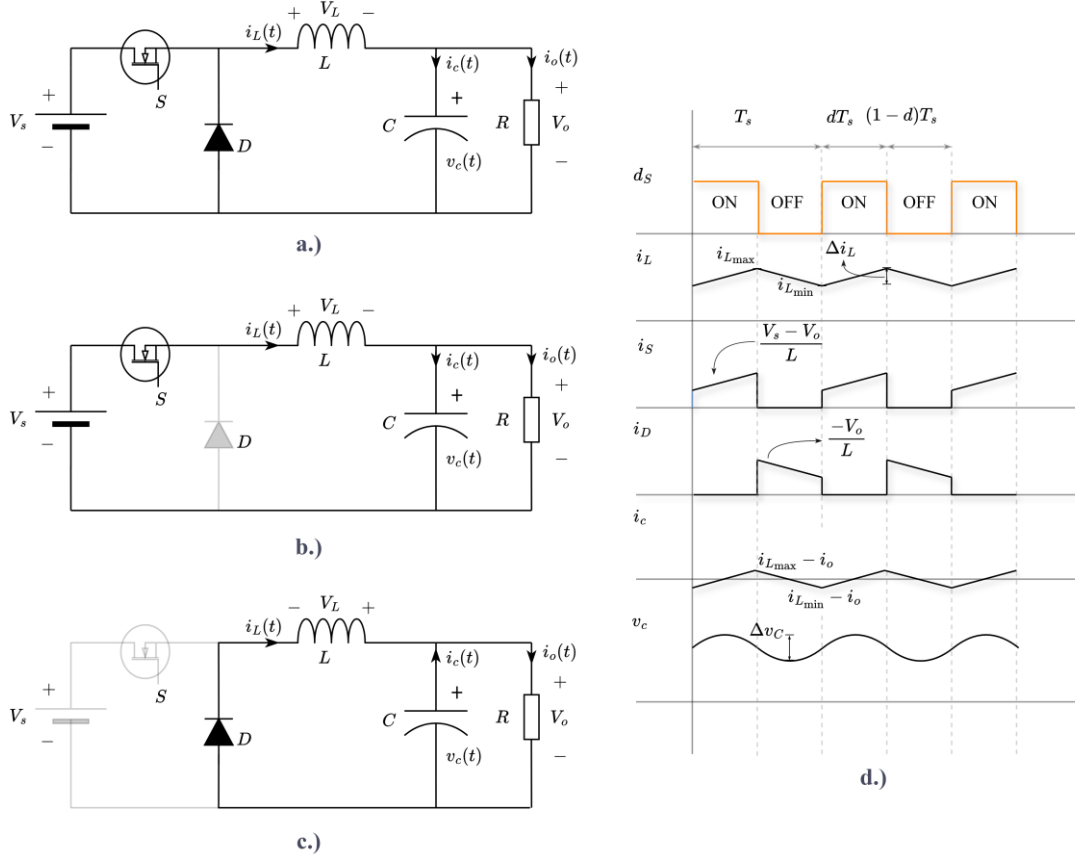


Figure 5. Buck converter operating modes and waveforms

Buck converters consist of an inductor (L) to ensure the continuity of the load current (i_o), a power MOSFET (S) positioned between the source (V_s) and the load (R) to adjust the load voltage (V_o), a diode (D) that will work complementarily with this MOSFET and a capacitor (C) to prevent load voltage ripples. The equivalent circuit of a conventional buck converter is shown in Figure 5a. As in conventional DC-DC power converters, the operation of the buck converter is examined in two modes. These modes are determined by the on and off states of the switch S .

$$L \frac{di_L(t)}{dt} = V_s - (1 - d(t))V_c(t) \quad (10)$$

$$C \frac{dV_c(t)}{dt} = i_L(1 - d(t)) - \frac{V_c(t)}{R} \quad (11)$$

Mode 1 starts with the S switch turning on, as shown in Figure 5b, and theoretically, the inductor current is assumed to increase linearly (dT_s). Mode 2, shown in Figure 5c, starts when switch S completes its duty cycle. In this case, D is turned on. The switching between S and

D occurs immediately in simulation applications but requires a very short dead time interval (usually in the microsecond levels) in experimental applications. In this case, the inductor current is assumed to decrease linearly ($(1 - d)T_s$). In the buck converter circuit in Figure 5a, $\dot{x}(t) = [i_L(t) \quad V_c(t)]^T$ are the state variables. When the switching function d is considered, the state equations of the circuit are as in Equations 10 and 11.

The linear model of the DC-DC buck converter can be modeled in the MATLAB/Simulink simulation environment using Equations 10 and 11. In addition, using these equations, the state space matrices and transfer functions of the buck converter can be written as follows.

$$A = \begin{bmatrix} 0 & -1/L \\ 1/C & -1/RC \end{bmatrix}, B = \begin{bmatrix} 1/L \\ 0 \end{bmatrix} V_s, C = [0 \quad 1] \quad (12)$$

$$G(s) = \frac{V_s/LC}{s^2 + (1/RC)s + 1/LC} \quad (13)$$

3.1. Buck Converter Design

Power converters are generally examined in two operating modes, namely continuous conduction mode (CCM) and discontinuous conduction mode (DCM) [39]. In Mode 1 in CCM, the load power is supplied by the input source, while it is supplied by the inductor only in Mode 2. In DCM, Mode 1 occurs the same way as CCM, but the load power drops to zero in Mode 2. The charging current and voltage should be continuous in power converters operating in energy storage systems. Otherwise, thermal problems will likely occur in battery cells exposed to intermittent charging currents. Therefore, the minimum values of the passive elements operating the battery and ultracapacitor in CCM mode must be determined. While determining these values, some assumptions are made for the fluctuation levels of the inductor current, capacitor voltage, and switching frequency. The manufacturer provides the charging and discharging current limits of the battery cells. In these values, charging limits are usually $1C$, while discharging limits can go up to $10C$ [32]. The C value is used to express battery capacities and is defined as the discharge current that will discharge a fully charged battery in 1 hour. Considering the electrical properties of the battery cell used in our study, the maximum charge current should be limited to $1C$ ($2500mA$). If the charge voltage is $4.2V$, the converter output power (P_o) should be $10.5W$. When switching and conduction losses are considered, it can be said that a converter with a power of $15W$ will be sufficient. Assuming that the ripple in the inductor current (Δi_L) in Figure 5d is $0.2A$ (this value is usually between 20% and 40% of the output current), the ripple in the capacitor voltage (Δv_C) is $2mV$, and the switching frequency (f_s) is $100kHz$, the filter inductor and capacitor values can be calculated as follows.

$$L_j = \frac{V_o(V_s - V_o)}{f_s \Delta i_L V_s}, j \in \{bat, uc\} \quad (14)$$

$$C_j = \frac{\Delta i_L}{8f_s \Delta v_C}, j \in \{bat, uc\} \quad (15)$$

According to Equations 14 and 15, converter inductances $L = 0.682mH$ and capacitances $C = 30\mu F$ were selected considering converter losses. The values of passive elements should be selected higher than the calculated minimum values, considering the operating conditions of the converter at a very low duty ratio.

Table 3. Electrical parameters of the buck converters

Parameter	Description	Value	Unit
V_s	Input voltage	12	V
L	Inductance	0.628	mH
C_{dc}	DC link Capacitance	30	μF
R_{dc}	DC link resistance	200	$k\Omega$
f_s	Switching frequency	100	kHz

Especially in buck converters with intermittent input current, operating conditions at high switching frequencies and low duty ratios may disrupt the continuity

of the output current. Therefore, it should not be forgotten that the calculated passive element values are the critical values required to provide the specified conditions. In this study, the electrical parameters of the single-input multi-output buck converter designed at the same power for battery and ultracapacitor synchronous charging are given in Table 3. The DC link resistance (R_{dc}), not included in the design phase in Table 3, prevents the output current from dropping to zero when the battery or ultracapacitor cell is disconnected from the charging terminal. If not, the output voltage increases excessively, creating a safety risk. The R_{dc} , limits the voltage by keeping the converter output current at a minimum level, eliminating this risk.

3.2. Cascade Control of Cascade Buck Converter for Proposed Synchronous Charge Architecture

In charging applications of energy storage devices, cell voltage and current must be controlled separately. This process is achieved by the CC-CV charging technique, which is frequently used to extend the battery's service life and increase charging efficiency [40]. Power electronic converters are usually controlled by average voltage or current control. However, terminal voltage may reach dangerous limits in energy storage systems if only current control is performed. Similarly, when only voltage control is performed, unlimited cell current may cause irreversible damage to the physical and chemical properties of the cell [41]. Compared to ultracapacitors, the critical control limits mentioned above are more effective in battery cells. Since ultracapacitors have high power density, they can withstand high charging currents without compromising their cycle life and physical properties. Since the battery and the ultracapacitor cell will be charged synchronously in this study, the buck converter designed in Section 4.1 was modified to be single-input and multi-output. Figure 6 shows the general structure of the system designed for synchronous charging. The power stage is formed by cascading two buck converters in such a way that the input voltages are the same and the output voltages are different. Detailed information on the implementation of the Cascade control structure for power converters can be found in the following reference [13]. The outputs of the converters are connected to the battery and ultracapacitor cells, respectively. The control algorithms implemented for cascade control of the relevant converter are shown in the upper part of the battery converter and the lower part of the ultracapacitor converter. In both control flows, the input reference voltages ($V_{j,ref}, j \in \{bat, uc\}$) are cell charge limit voltages [42]. The reference voltages are compared with the cell voltages, and a reference current value is generated to adjust the charge current. This value is limited by the maximum charge and discharge currents provided by the manufacturer with dynamic saturation. Ultracapacitors can withstand much higher charge currents than this limit current. However, the battery and ultracapacitor currents were selected with closer amplitudes for the synchronous charging application carried out in this study. The dynamic saturation generates the reference charge current ($I_{j,ref}, j \in \{bat, uc\}$), which is compared with the output current.

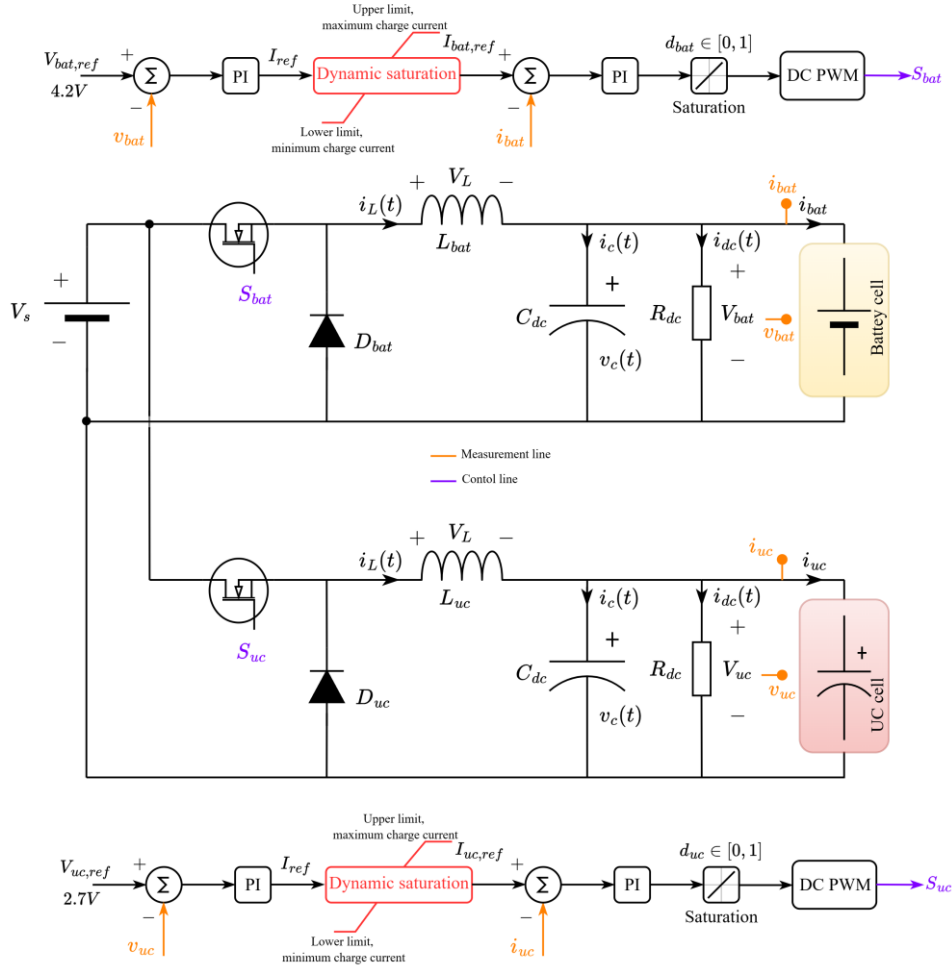


Figure 6. Overall architecture of synchronous charge of battery and ultracapacitor cells

The output of the second controller used to eliminate the current error produces the converter duty ratio required to provide the given reference values. In the control algorithm, the inner loop controls the charge currents while the outer loop controls the charge voltages. Therefore, cascade control is achieved by controlling more than one output variable. In the cascade buck converter in Figure 6, since the capacitor current (i_c) and the protection resistor current (i_{dc}) are negligibly small in CCM, the output current (i_{bat}) can be assumed to be equal to the inductor current (i_L). The transfer function between the input variable duty ratio (d) and the output variable inductor current (i_L) can be given as follows [43].

$$G_{id}(s) = \frac{i_L(s)}{d(s)} = \frac{V_s}{dR} \left(\frac{1 + sRC}{s^2LC + (L/R)s + 1} \right) \quad (16)$$

Similarly, the transfer function between the input variable duty ratio (d) and the output variable battery voltage (V_{bat}) can be given as follows [44].

$$G_{vd}(s) = \frac{v_c(s)}{d(s)} = \frac{V_s}{d} \left(\frac{1}{s^2LC + (L/R)s + 1} \right) \quad (17)$$

Controller design can be performed using the pidTuner toolbox in the MATLAB environment using Equations 16

and 17. For this study, the proportional integral (PI) controller structure, which is used in many applications due to its simple structure and robustness, was preferred. The PI controller transfer function is:

$$G_{PI}(s) = K_p \left(1 + \frac{1}{T_i s} \right) \quad (18)$$

In Equation 18, K_p represents the proportional gain, and T_i represents the integral time constant. When implementing the cascade control structure, it should be considered that the inner control loops (current control) will change much faster than the outer control loops (voltage control). For this reason, the integral time of the inner control loops is selected 5 to 10 times smaller than the outer control loops.

4. RESULT AND DISCUSSION

To prove the effectiveness of the proposed technique, the synchronous charging architecture consisting of a battery, ultracapacitor, and buck converter components, the details of which are shown in Figure 6, were modeled in the MATLAB/Simulink environment. The results were obtained separately since the energy storage devices are charged independently. Similar charging procedures were created for both the battery and the ultracapacitor cells. The charging procedure of the battery cell can be

summarized as follows: In the first step, a charging current of $0.2C$ is given to the battery cell as a reference. In the following steps, this rate is increased by $0.2C$ every $0.5s$ by giving sufficient rest periods to the battery cell until the battery cell reaches the maximum charging current. When the charging current reaches the maximum level ($1C = 2500mA$ for the battery cell used in this study), this current level is maintained until the battery is in continuous voltage mode. The simulation results of the battery cell are shown in Figure 7. Figure 7a shows the SoC change of the battery cell during the test procedure. The battery cell started the charging process from the

initial SoC level of 50% and was charged to approximately 50.25% at the end of the simulation. Increasing the charging current at the beginning of the charging process caused a slow change in the SoC. However, it is seen that the charging speed increases when the charging current reaches $1C$. The reason for the very low increase in the battery SoC is due to the short test period. The simulation period was kept short to show the cell changes during charging clearly. The change in the battery terminal voltage according to the reference charging currents is shown in Figure 7b.

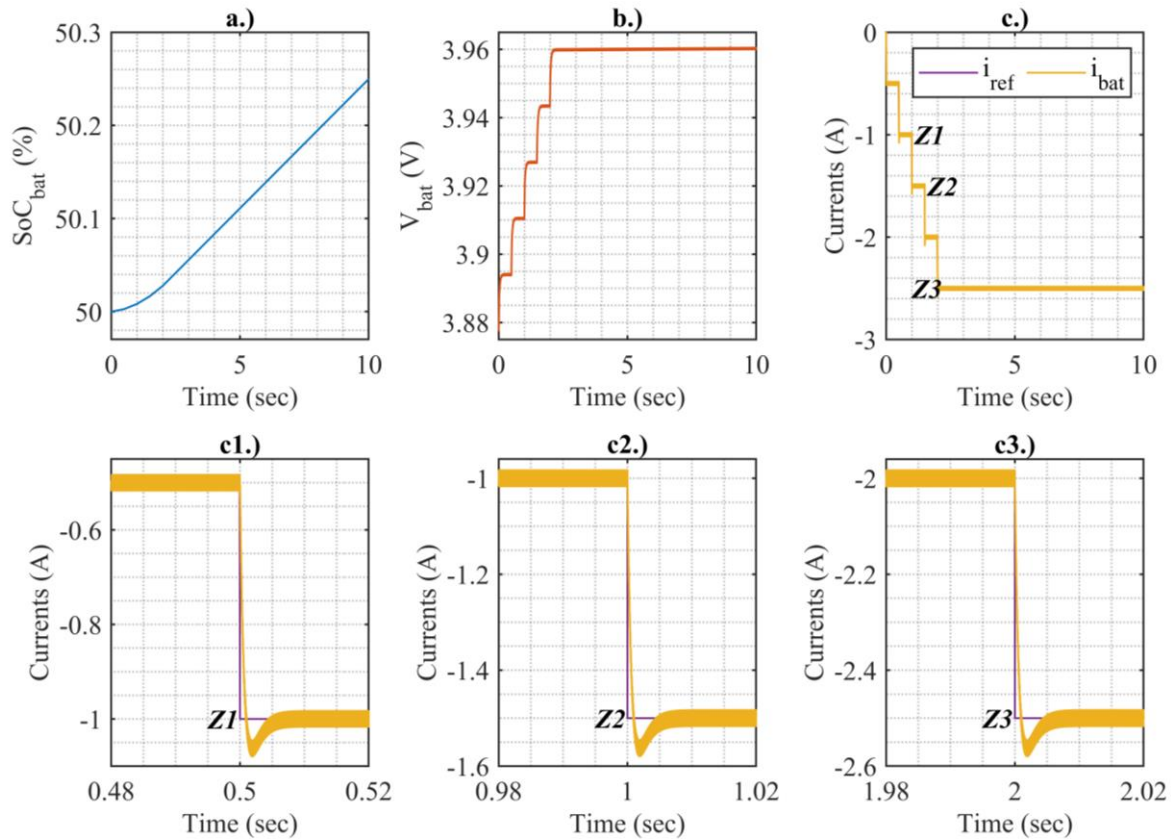


Figure 7. Simulation results of battery cell, a.) SoC, b.) Terminal voltage, c.) Battery current and reference current (c1.), c2.), and c3.) are zoom of c.) at Z1, Z2, and Z3 regions)

Two increasing effects are seen on the battery terminal voltage in parallel with the increase in the charging current. The first is the increase in the internal resistance voltage with the increase in the current passing through the battery's internal resistance. The second is due to the increased battery potential due to the charged Lithium ions passing to the cathode side under the effect of the charging current. The reason for the gradual increase in terminal voltage is directly related to the change in battery charging current. The changes in terminal voltage after each charging pulse were measured as 3.893V, 3.910V, 3.926V, 3.943V, and 3.960V. In Figure 7c, the reference charging current and battery charging current are shown in the same graph. The charging current was applied at times $(t = k, \{k \in 0, 0.5, 1, 1.5, 2\})$ and $(i_{ref} = n, \{n \in 0.2C, 0.4C, 0.6C, 0.8C, 1C\})$, respectively. This procedure aims to test the robustness of the designed cascade control system. Since the simulation time is short

and the charging current is changed in a very narrow interval, Figure 7c was examined closely at three different points (Z1, Z2, Z3) in order to clearly show the battery current tracking states of the reference. The specified Z1, Z2, Z3 regions are shown closely in Figure 7c1, Figure 7c2 and Figure 7c3, respectively, as an extension of Figure 7c. In all three results, it is seen that the charging current reaches the reference value in a very short time and closely follows the reference with a very small overshoot. For the examined Z1, Z2 and Z3 regions, the overshoot values are measured as 7.939%, 7.944%, 7.953%, and the settling times are approximately 6ms. These values prove the buck converter's accuracy and the adopted control method. In addition, to test the suitability of both the design values and the control algorithm for the buck converter, the time-dependent changes of the effective duty ratio (d_{bat}), diode current ($i_{D,bat}$), and MOSFET current ($i_{fet,bat}$) during the charging process

are shown in Figure 8. Zoomed images are given on the right side of the relevant graph in a short period of time interval when the reference charging current is $0.3C$ to closely monitor the changes on the converter side during the test. Figure 8a shows the change in the duty ratio. At the beginning of the charging process, the effective duty ratio is captured quickly and robustly. The increase in the duty ratio because of the change in the charging currents can be observed in the range of $0 < t < 2$ seconds and increases with time when the charging current is fixed at $1C$. This is because the battery cell terminal voltage (i.e.

converter output voltage) continues to increase during the charging period. Figure 8b and Figure 8c show the converter diode and MOSFET currents, respectively. When looking at the zoomed-in view of Figure 8b, it is seen that the diode current is zero during the duty cycle and carries the reference current in the regions outside the duty cycle ($1 - d$). Since the diode and MOSFET in the converter structure work in complementary to each other, it is expected that the reference current will be seen on the MOSFET during the duty cycle. Figure 8c proves this expected situation.

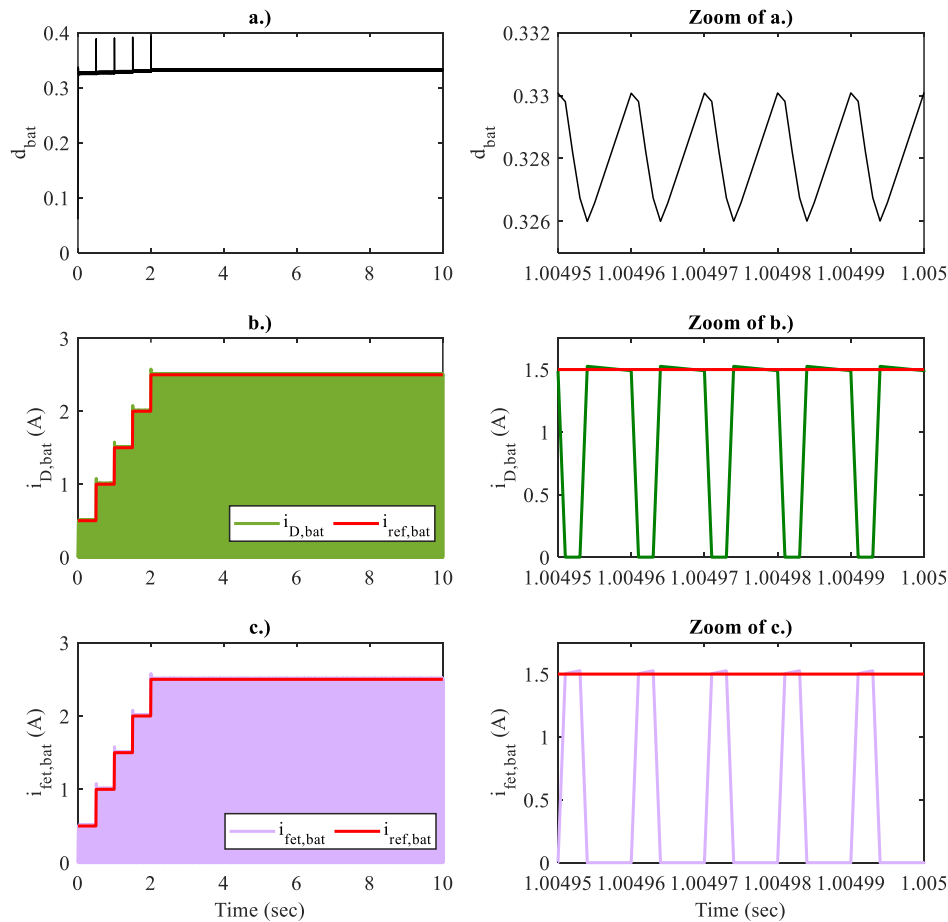


Figure 8. Results of battery buck converter, a.) Duty cycle, b.) Reference and diode current, c.) Reference current and MOSFET current

The results in Figure 7 and Figure 8 mainly focus on the current control, which is the inner loop of the designed cascade control system. The robustness of the voltage control, which constitutes the outer loop of the control system, can be tested when the cell terminal voltage reaches the charging voltage or when the battery cell is charged with a higher than the nominal charging voltage. During charging, the cell terminal voltage increases almost linearly to approximately 80% SoC. It is clear that the cell is charged in the continuous current (CC) mode in this region. The charging current starts to decrease when the cell terminal voltage reaches the charging voltage. After this decrease, the charging process continues in the continuous voltage (CV) mode. In order to test the effectiveness of the outer loop control mechanisms, a second simulation procedure was applied by starting the battery cell SoC from 80%. In this procedure, the minimum value of the charging current was selected as $0.4C$ and the maximum value as $3.2C$. The charging

current comprises pulses with a period of 0.3s and a duty cycle of 80%. Figure 9 shows the changes in the battery cell exposed to these pulses. The time-dependent change of the charge currents (i_{ch}) is shown in Figure 9a. Figure 9b shows the change of the battery cell current depending on the application of the charge currents. As can be seen, despite applying a charge current of 8A at $t = 0$, the external loop control mechanisms have successfully ensured that the terminal voltage does not exceed the specified limit value and have started to reduce the charging current. In this case, the battery cell continues to charge in CV mode. Afterward, the charge current is reduced to 1A, and the CC mode is observed, where the charging process continues continuously at this value. Figure 9c and Figure 9d show the battery terminal voltage and the battery SoC, respectively. Limiting the battery terminal voltage against high charging currents again demonstrates the robustness of the control system.

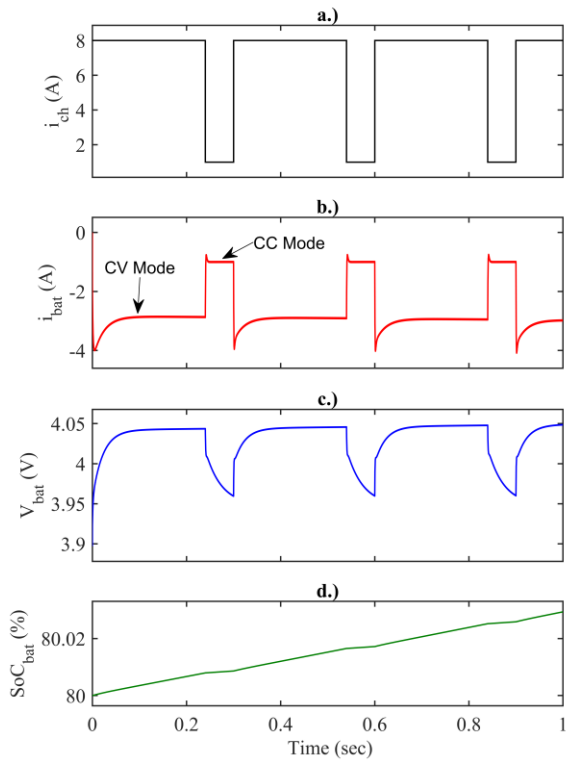


Figure 9. Test results of designed control algorithm in Continuous Current (CC) and Continuous Voltage (CV) modes for battery cell

The charging procedure of the ultracapacitor cell was applied similarly to the charging procedure of the battery cell. The only difference was that the charging currents were selected 0.2A lower than the battery cell, considering that the ultracapacitor cell would charge very quickly. Therefore, the ultracapacitor charging current

was applied at times $(t = k, \{k \in 0, 0.5, 1, 1.5, 2\})$ and $(i_{ref} = n, \{n \in 0.3A, 0.8A, 1.3A, 1.8A, 2A\})$, respectively. Figure 10 shows the simulation results of the ultracapacitor cell. The ultracapacitor SoC shown in Figure 10a started with a charge rate of approximately 50% and reached approximately 75% SoC at the end of the test. Since the SoC of the ultracapacitor cells is directly proportional to the terminal voltage, it is expected that the response in the SoC is similar to the cell voltage in Figure 10b. The reason why the ultracapacitor voltage increases linearly depending on the charging current is due to the use of electrostatic principles in the energy storage process. Unlike batteries, since no electrochemical transformation occurs, the dynamics in the cell voltage are more linear. The ultracapacitor voltage was measured as 1.512V at $t = 0$ and 2.229V at the end of the charging process. The time-dependent change of the selected reference current (i_{ref}) and ultracapacitor current (i_{uc}) in the ultracapacitor charging process is shown in Figure 10c. Since the simulation time is short and the charging current is changed in a very narrow range, Figure 10c was examined closely at three different points (Z4, Z5, Z6) in order to show the reference tracking states of the ultracapacitor current clearly. The specified regions Z4, Z5, and Z6 are shown closely in Figure 10c1, Figure 10c2, and Figure 10c3, respectively, as an extension of Figure 10c. In all three results, it is seen that the charging current reaches the reference value in a very short time and follows the reference closely with a very small overshoot. For the examined Z4, Z5, and Z6 regions, the overshoot values are measured as 7.281%, 7.288% , 7.312% , and the settling times are approximately 6ms.

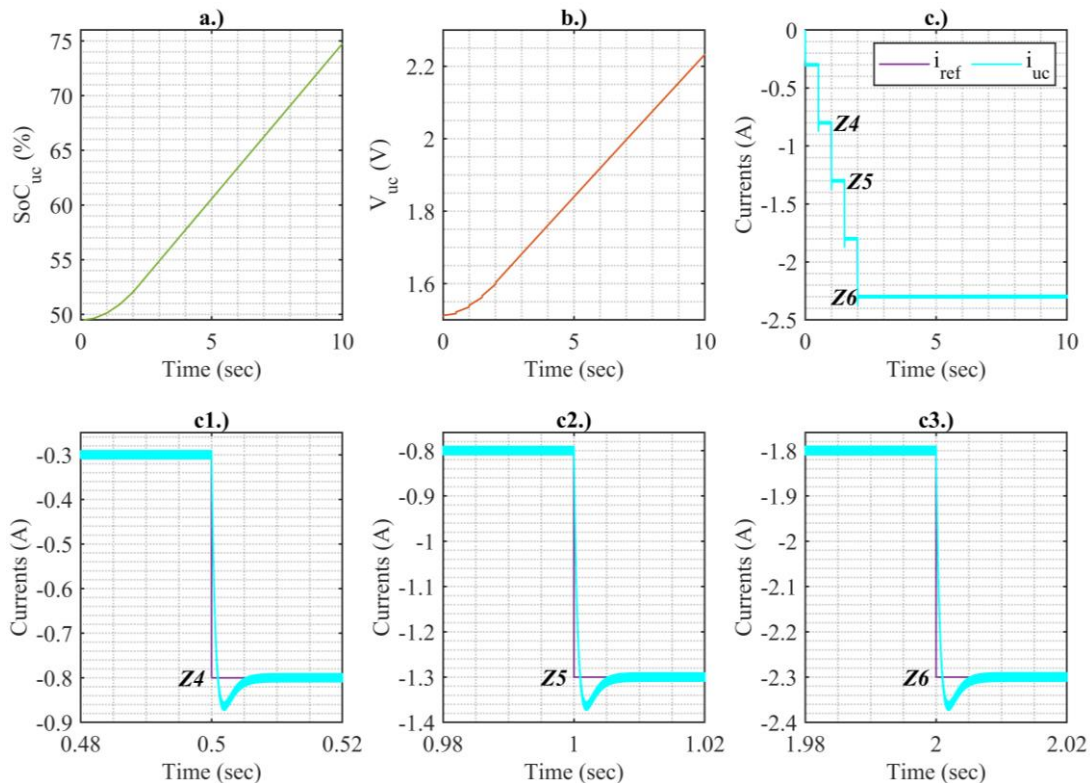


Figure 10. Simulation results of ultracapacitor, a.) SoC, b.) Terminal voltage, c.) Battery current and reference current (c1.), c2.), and c3.) are zoom of c.) at Z4, Z5, and Z6 regions)

Figures 11a, 11b and 11c show the time-dependent changes of the duty ratio (d_{uc}), diode current ($i_{D,uc}$), and MOSFET current ($i_{fet,uc}$) of the ultracapacitor converter, respectively. In order to closely monitor the changes on

the converter side during the test, close-up images of a short region of the time interval when the reference charge current is 1.3A are given on the right side of the relevant graph.

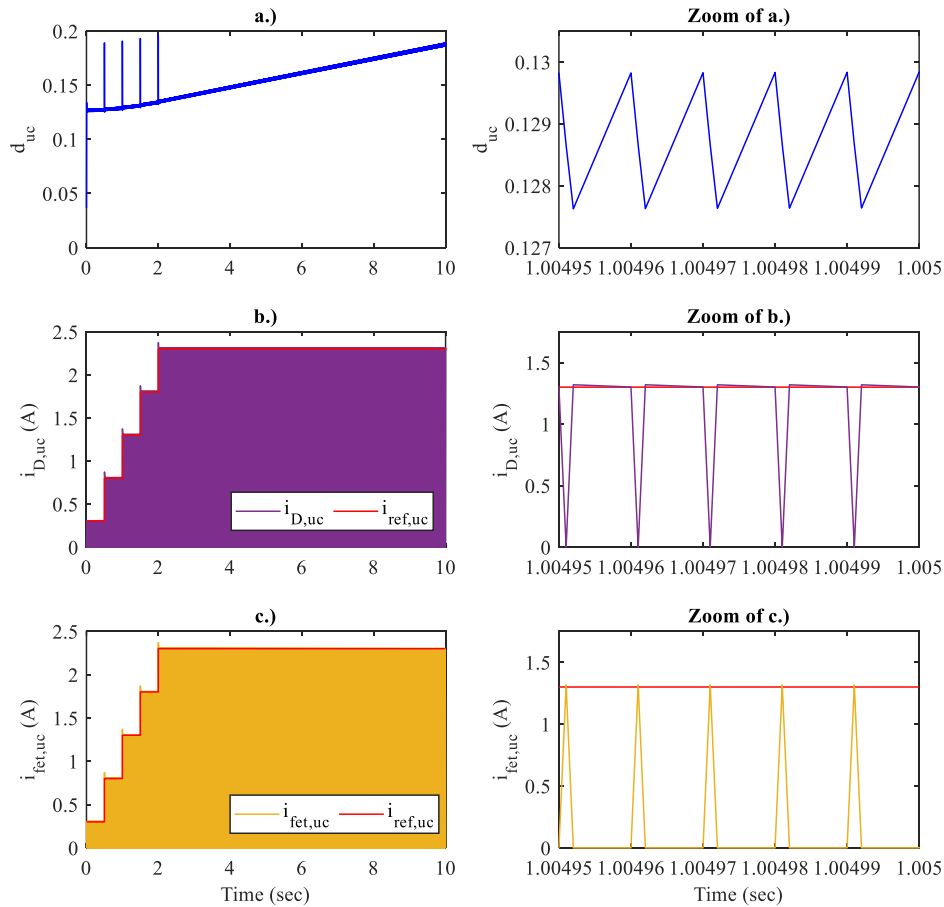


Figure 11. Results of ultracapacitor buck converter, a.) Duty cycle, b.) Reference and diode current, c.) Reference current and MOSFET current

It is seen that the duty ratio in Figure 11a increases linearly. This is due to the rapid increase in the ultracapacitor cell voltage. It is seen that the peaks in the duty cycle in current changes are very short time, and the control algorithm quickly tracks the duty ratio. It is expected that similar effects are seen in the diode current in Figure 11b and the MOSFET current in Figure 11c as in the battery cell. The difference is that the charge reference current is 0.2A lower for the ultracapacitor tests. Although the charge currents differ, the reference currents can be closely monitored thanks to the superior success of the designed control algorithm. Similar to the test procedure of the battery cell, the ultracapacitor converter controls the external loop mechanisms so that the cell limit voltage is not exceeded. Therefore, charging current increasing the cell voltage above the nominal voltage is not allowed. To check the external loop mechanisms of the ultracapacitor, a second test procedure was performed by starting the cell SoC from 80%. This procedure is the same as the second procedure for the battery cell. Figure 12 shows the test results of the inner (cell current control) and outer (cell voltage control) control mechanisms. Figure 12a shows the reference pulsed charging current effective at 80% at a maximum of 8A and a minimum of 1A. The cell current (i_{uc}), cell

voltage (V_{uc}) and state of charge (SoC_{uc}) in the ultracapacitor cell under the influence of these charging currents are shown in Figures 12b, 12c and 12d, respectively. It is observed that the charging current gradually decreases by increasing the cell voltage close to the nominal voltage, thanks to the effective operation of the external loop mechanisms (CV Mode). As the charging current is reduced to 1A, the terminal voltage drops rapidly, and the charging current becomes continuous (CC Mode).

Today, most electric vehicles use only battery packs as energy storage devices. Hybrid electric vehicles use battery packs as auxiliary energy sources, while fully electric vehicles use them as the primary energy source. In renewable energy systems, battery packs are indispensable energy storage and supply devices. In hybrid power systems containing battery/ultracapacitors, ultracapacitors meet peak currents and prevent thermal and cycle life problems of battery packs. Ultracapacitors must be operated within a specific SoC range to meet the peak currents demanded by the load as both source and storage device. Ultracapacitors can fulfill this mission by storing either the energy of the battery packs or the recovered energy originating from the load. However,

while sharing the battery energy with the ultracapacitor can cause the battery SoC to decrease rapidly, the ultracapacitor cannot meet the peak currents if insufficient recovered energy exists. Therefore, charging the ultracapacitor to a specific SoC while the battery is charging will prepare the system for power supply and energy storage.

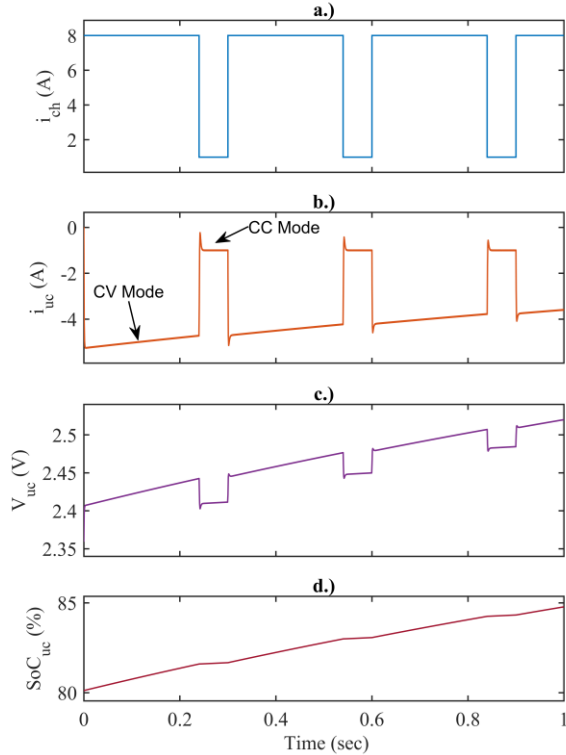


Figure 12. Test results of designed control algorithm in Continuous Current (CC) and Continuous Voltage (CV) modes for ultracapacitor cell

4. CONCLUSION

In the near future, when hybrid power systems using more than one energy storage device are widespread, the process of charging these devices separately will come to light. Especially in battery/ultracapacitor systems, which have been the subject of a serious research attack in recent years, the synchronous charging process may be of vital importance in terms of charging time. In this study, a battery and ultracapacitor synchronous charging system has been developed for small power applications. Although all simulation tests have been performed at cell size, the proposed system can easily be applied to larger-volume hybrid power systems. The superior success of the designed buck converter in capturing the reference charging currents proves that the critical calculations of the control algorithm are performed effectively. In addition, the designed control structure has shown superior success in obtaining both medium-level duty ratios (battery cell test) and low-level duty ratios (ultracapacitor cell test). In addition, the proposed synchronous charging system has provided serious performance by monitoring all reference charging currents with approximately 8% overshoot and 6ms settling time. The obtained results prove the applicability of the cascading control technique implemented in the

buck converter structure in both continuous current and continuous voltage modes. In future studies, it is planned to realize a cell-sized hardware prototype for HESS containing battery and ultracapacitor cells using the technique proposed in this study.

REFERENCES

- [1] Emrani A and Berrada A, A comprehensive review on techno-economic assessment of hybrid energy storage systems integrated with renewable energy, *Journal of Energy Storage*. 2024; 84, 111010.
- [2] Kaan M, Bozkurt A, Genç M S, and Genç G, Optimization study of an energy storage system supplied solar and wind energy sources for green campus, *Process Safety and Environmental Protection*. 2024; 190, 863-872.
- [3] Zhu Z *et al.*, Versatile carbon-based materials from biomass for advanced electrochemical energy storage systems, *eScience*. 2024; 4, 5, 100249.
- [4] Tian J, Fan Y, Pan T, Zhang X, Yin J, and Zhang Q, A critical review on inconsistency mechanism, evaluation methods and improvement measures for lithium-ion battery energy storage systems, *Renewable and Sustainable Energy Reviews*. 2024; 189, 113978.
- [5] Nivolianiti E, Karnavas Y L, and Charpentier J-F, Energy management of shipboard microgrids integrating energy storage systems: A review, *Renewable and Sustainable Energy Reviews*. 2024; 189, 114012.
- [6] Robles-Campos H R, Valderrabano-Gonzalez A, Rosas-Caro J C, Gabbar H A, and Babaiahgari B, Double Dual High Step-Up Power Converter with Reduced Stored Energy, *Energies*. 2023; 16, 7, 3194.
- [7] Çorapsız M R, PV-fed multi-output buck converter-based renewable energy storage system with extended current control for lifetime extension of Li-ion batteries, *Computers and Electrical Engineering*. 2024; 120, 109757.
- [8] Çorapsız M R and Kahveci H, Double adaptive power allocation strategy in electric vehicles with battery/supercapacitor hybrid energy storage system, *International Journal of Energy Research*. 2022; 46, 13, 18819-18838.
- [9] Usvarman R, Munawar K, Ramli M A M, and Mehedi I M, Bus Voltage Stabilization of a Sustainable Photovoltaic-Fed DC Microgrid with Hybrid Energy Storage Systems, *Sustainability*. 2024; 16, 6, 2307.
- [10] Çorapsız M R and Kahveci H, A study on Li-ion battery and supercapacitor design for hybrid energy storage systems, *Energy Storage*. 2023; 5, 1, e386.
- [11] Chakraborty S, Hasan M M, Worighi I, Hegazy O, and Razzak M A, Performance Evaluation of a PID-Controlled Synchronous Buck Converter Based Battery Charging Controller for Solar-Powered Lighting System in a Fishing Trawler, *Energies*. 2018; 11, 10, 2722.
- [12] López-Santos O *et al.*, Robust Control for a Battery Charger Using a Quadratic Buck Converter, *IEEE Access*. 2024; 12, 125480-125492.

- [13] Florescu A, Bacha S, Munteanu I, Bratcu A I, and Rumeau A, Adaptive frequency-separation-based energy management system for electric vehicles, *Journal of Power Sources*. 2015; 280, 410-421.
- [14] Yılmaz M, Kaleli A, and Çorapsız M F, Machine learning based dynamic super twisting sliding mode controller for increase speed and accuracy of MPPT using real-time data under PSCs, *Renewable Energy*. 2023; 219, 119470.
- [15] Kushwaha R and Singh B, A Power Quality Improved EV Charger With Bridgeless Cuk Converter, *IEEE Transactions on Industry Applications*. 2019; 55, 5, 5190-5203.
- [16] Singh K, Anand A, Mishra A K, Singh B, and Sahay K, SEPIC Converter for Solar PV Array Fed Battery Charging in DC Homes, *Journal of The Institution of Engineers (India): Series B*. 2021; 102, 3, 455-463.
- [17] Acosta L N and Flexer V, Accelerated charging protocols for lithium-ion batteries: Are fast chargers really convenient?, *Journal of Solid State Electrochemistry*. 2024; 28, 3, 1107-1119.
- [18] Wu Y *et al.*, Adaptive power allocation using artificial potential field with compensator for hybrid energy storage systems in electric vehicles, *Applied Energy*. 2020; 257, 113983.
- [19] Raut K, Shendge A, Chaudhari J, Lamba R, and Alshammari N F, Modeling and simulation of photovoltaic powered battery-supercapacitor hybrid energy storage system for electric vehicles, *Journal of Energy Storage*. 2024; 82, 110324.
- [20] Shen Y, Xie J, He T, Yao L, and Xiao Y, CEEMD-Fuzzy Control Energy Management of Hybrid Energy Storage Systems in Electric Vehicles, *IEEE Transactions on Energy Conversion*. 2024; 39, 1, 555-566.
- [21] Reddy R M, Das M, and Chauhan N, Novel Battery-Supercapacitor Hybrid Energy Storage System for Wide Ambient Temperature Electric Vehicles Operation, *IEEE Transactions on Circuits and Systems II: Express Briefs*. 2023; 70, 7, 2580-2584.
- [22] Snoussi J, Elghali S B, Benbouzid M, and Mimouni M F, Optimal Sizing of Energy Storage Systems Using Frequency-Separation-Based Energy Management for Fuel Cell Hybrid Electric Vehicles, *IEEE Transactions on Vehicular Technology*. 2018; 67, 10, 9337-9346.
- [23] Zuo W, Li R, Zhou C, Li Y, Xia J, and Liu J, Battery-Supercapacitor Hybrid Devices: Recent Progress and Future Prospects, *Advanced Science*. 2017; 4, 7, 1600539.
- [24] Watanabe S, Kinoshita M, Hosokawa T, Morigaki K, and Nakura K, Capacity fading of $\text{LiAl}_x\text{Ni}_{1-x}\text{Co}_y\text{O}_2$ cathode for lithium-ion batteries during accelerated calendar and cycle life tests (effect of depth of discharge in charge-discharge cycling on the suppression of the micro-crack generation of $\text{LiAl}_x\text{Ni}_{1-x}\text{Co}_y\text{O}_2$ particle), *Journal of Power Sources*. 2014; 260, 50-56.
- [25] Trovão J P, Silva M A, and Dubois M R, Coupled energy management algorithm for MESS in urban EV, *IET Electrical Systems in Transportation*. 2017; 7, 2, 125-134.
- [26] Castaings A, Lhomme W, Trigui R, and Bouscayrol A, Comparison of energy management strategies of a battery/supercapacitors system for electric vehicle under real-time constraints, *Applied Energy*. 2016; 163, 190-200.
- [27] Usman Tahir M, Sangwongwanich A, Stroe D-I, and Blaabjerg F, Overview of multi-stage charging strategies for Li-ion batteries, *Journal of Energy Chemistry*. 2023; 84, 228-241.
- [28] Saxena S, Le Floch C, MacDonald J, and Moura S, Quantifying EV battery end-of-life through analysis of travel needs with vehicle powertrain models, *Journal of Power Sources*. 2015; 282, 265-276.
- [29] Roy P and Srivastava S K, Nanostructured anode materials for lithium ion batteries, *Journal of Materials Chemistry A*. 2015; 3, 6, 2454-2484.
- [30] Lu Y, Zhang Q, Li F, and Chen J, Emerging Lithiated Organic Cathode Materials for Lithium-Ion Full Batteries, *Angewandte Chemie*. 2023; 135, 7, e202216047.
- [31] Campagna N *et al.*, Battery Models for Battery Powered Applications: A Comparative Study, *Energies*. 2020; 13, 16, 4085.
- [32] URL-1, ORION 18650P/25 2500mAh 10C. <https://static.ticimax.cloud/37661/uploads/dosyalar/orion18650p250010.pdf> (accessed 31.10.2024).
- [33] Miller J R and Simon P, Electrochemical Capacitors for Energy Management, *Science*. 2008; 321, 5889, 651-652.
- [34] Drummond R, Huang C, Grant P S, and Duncan S R, Overcoming diffusion limitations in supercapacitors using layered electrodes, *Journal of Power Sources*. 2019; 433, 126579.
- [35] González A, Goikolea E, Barrera J A, and Mysyk R, Review on supercapacitors: Technologies and materials, *Renewable and Sustainable Energy Reviews*. 2016; 58, 1189-1206.
- [36] Zubieta L and Bonert R, Characterization of double-layer capacitors for power electronics applications, *IEEE Transactions on Industry Applications*. 2000; 36, 1, 199-205.
- [37] URL-2, Maxwell Ultracapacitor Cell. <https://maxwell.com/products/ultracapacitors/cells/> (accessed 10.01.2025).
- [38] Sani S G, Banaei M R, and Hosseini S H, Investigation and implementation of a common ground DC-DC buck converter with a novel control method for loss reduction in the converter, *IET Power Electronics*. 2024; 17, 14, 1840-1851.
- [39] Kim H C, Biswas M, and Park J W, Discontinuous Conduction Mode Analysis of Two-Phase Interleaved Buck Converter With Inversely Coupled Inductor, *IEEE Access*. 2024; 12, 91944-91956.
- [40] He L, Wang X, and Lee C-K, A Study and Implementation of Inductive Power Transfer System Using Hybrid Control Strategy for CC-CV Battery Charging, *Sustainability*. 2023; 15, 4, 3606.
- [41] Zhang S S, Identifying rate limitation and a guide to design of fast-charging Li-ion battery, *InfoMat*. 2020; 2, 5, 942-949.

- [42] Kollimalla S K, Ukil A, Gooi H B, Manandhar U, and Tummuru N R, Optimization of Charge/Discharge Rates of a Battery Using a Two-Stage Rate-Limit Control, *IEEE Transactions on Sustainable Energy*. 2017; 8, 2, 516-529.
- [43] Argyrou M C, Marouchos C C, Kalogirou S A, and Christodoulides P, Modeling a residential grid-connected PV system with battery–supercapacitor storage: Control design and stability analysis, *Energy Reports*. 2021; 7, 4988-5002.
- [44] Hong X, Wu J-F, and Wei C-L, 98.1%-Efficiency Hysteretic-Current-Mode Noninverting Buck–Boost DC-DC Converter With Smooth Mode Transition, *IEEE Transactions on Power Electronics*. 2017; 32, 2008-2017.